Proceedings of the XLIInd RENCONTRES DE MORIOND

Gravitational Waves and Experimental Gravity

La Thuile, Val d'Aoste, Italie March 11 - 18, 2007

# 2007
# Gravitational Waves and Experimental Gravity

edited by

Jacques Dumarchez
and
Jean Trân Thanh Vân

THẾ GIỚI

PUBLISHERS

# STATUS REPORT ON THE MEASUREMENT OF THE CASIMIR FORCE IN A CYLINDER-PLANE GEOMETRY

Woo-Joong Kim[a], Michael Brown-Hayes[a], Diego A.R. Dalvit[b], and Roberto Onofrio[a,c]
[a] *Department of Physics and Astronomy, Dartmouth College, Hanover, NH 03755, USA*
[b] *Theoretical Division, Los Alamos National Laboratory, Los Alamos, NM 87545, USA*
[c] *Dipartimento di Fisica "Galileo Galilei", Università di Padova, Via Marzolo 8, 35131 Padova, Italy*

We report on an ongoing experimental effort to measure the Casimir force in the cylinder-plane geometry. The experimental technique and some of the recent results are described, with particular emphasis on the electrostatic calibrations of both the cylinder-plane and the sphere-plane geometries.

## 1 Introduction

Experimental and theoretical studies of Casimir forces [1] have become of growing importance due to their potential role both in cosmology [2,3] as a candidate for propelling the observed acceleration of the universe, [4] and in experimental gravitation since Casimir forces provide the leading expected background to hypothetical short-range forces of gravitational origin conjectured in various unification models.[5] An increasing number of demonstrations of the Casimir force have been realized in various geometries,[6] which represent significant progress with respect to the pioneering measurements [7] (for more detailed accounts on theory and experiment see for instance [8,9] and [10] respectively). Precision studies of the Casimir forces, which may allow for a better control of residuals to seek novel forces, in all the room-temperature experiments performed so far, are currently limited by the presence of the thermal photons which manifest themselves in addition to the zero-point photons responsible for the genuine Casimir pressure.[11] The thermal effect, non trivial in the simultaneous presence of finite conductivity corrections,[12] is difficult to measure in the sphere-plane configuration due to the fast drop in the overall Casimir signal at the distances for which the thermal photons should result in a significant correction to the overall force in the 1-8 $\mu$m range. On the other hand, for the parallel plate configuration, the parallelism requirements are quite stringent and demand a complex control system.[13] Recently, it has been proposed to study the Casimir force in the cylinder-plane configuration, [14] and a first prototype has been built and calibrated.[15] The outcome of these preliminary studies showed that the Casimir force in the cylinder-plane configuration should provide a signal large enough to detect the effect of the thermal photons, while simplifying the control of parallelism with respect to the parallel-plane case. Moreover, various recent theoretical analysis have shown that this geometry is interesting in itself [16] with particular regard to the existence of exact solutions that could allow for the test of the Proximity Force Approximation [17,18] (PFA) used in all the non-planar experiments performed so far, and considered to be the source of systematic errors in the theory-experiment comparison. In this report, we describe the current status of our experiment with particular focus on various systematic challenges associated with the measurement.

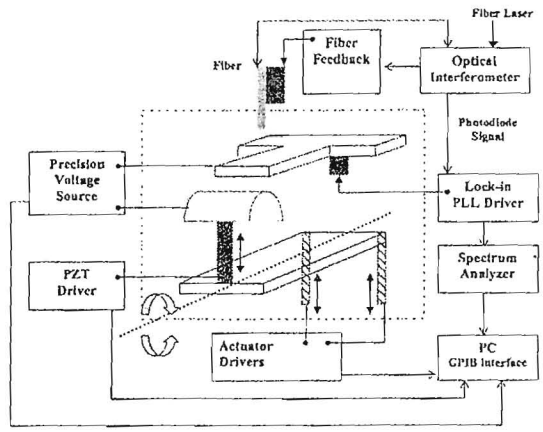


Figure 1: Schematic of the current experimental setup. A rectangular silicon cantilever of size 2cm × 1cm × 356$\mu$m is driven with a positive feedback by a phase-locked loop. The cantilever is electrically isolated and thermally stabilized by a Peltier cooler. Below the cantilever a cylindrical lens is mounted on a mechanical frame connected to two motorized actuators allowing for coarse translational motion if operated in common mode, or for parallelization when operated in differential mode. An additional piezoelectric transducer is installed for fine translational motion of the cylindrical lens.

## 2 Experimental set-up

The overall experimental setup is an upgrade on the one already described in a previous paper,[15] the main distinction being the use of a phase-locked loop scheme[19] to drive the cantilever at its resonant frequency. A schematic of the apparatus is shown in Fig. 1. A rectangular cantilever made from a laser cut silicon wafer provides the flat surface (with roughness measured at a scanning electron microscope to be less than 50 nm), facing a plano-convex cylindrical lens of radius of curvature $R = 20.7$ mm (with tolerance $\pm 1\%$), length $L = (20 \pm 0.1)$ mm, and width $w = (10 \pm 0.1)$mm. Assuming the density of silicon $\rho = 2.3 \times 10^3 \mathrm{kg/m^3}$, the physical mass of cantilever is $m = 1.64 \times 10^{-4}$ kg. Both the cylindrical lens and the surface of the cantilever are coated with a 200 nm layer of gold by thermal evaporation. The fundamental flexural mode of the cantilever at 886 Hz is detected by using a fiber optic interferometer fed by temperature stabilized diode lasers with an adjustable power in the 5-10 mW range. In different runs we have used two different lasers at the wavelengths of 670 nm and 770 nm. The output signal from the interferometer is filtered and amplified through a single reference mode lock-in amplifier and is fed back into the piezoelectric actuator driving the cantilever motion. The phase between the input and the output signals is properly chosen to maximize the oscillation amplitude, typically around 30-40 degrees. One of the advantages of this scheme is that the acquisition time for a single frequency measurement is significantly reduced with respect to the previous open-loop scheme in which a white noise was used as the driving source without a feedback, and the complete FFT spectrum was acquired. This gain may be quantified by estimating the effective bandwidth, typically in the 10 mHz range, corresponding to an effective mechanical quality factor of $Q_{\mathrm{eff}} \simeq 10^5$, to be compared to the quality factor measured in the open-loop configuration of the same resonance mode of $Q_0 \simeq 10^3$. We have noticed that the resonant frequency of the cantilever drifts as much as 2 Hz as the ambient temperature fluctuates about 1 K over the duration of a typical run of few hours. The effect of the thermal drifts has been mitigated at the direct hardware level by stabilizing the cantilever temperature with a Peltier cooler, and off-line by implementing a proper data acquisition sequence, as described below.

In order to calibrate the apparatus, a controllable electrostatic force is generated by applying

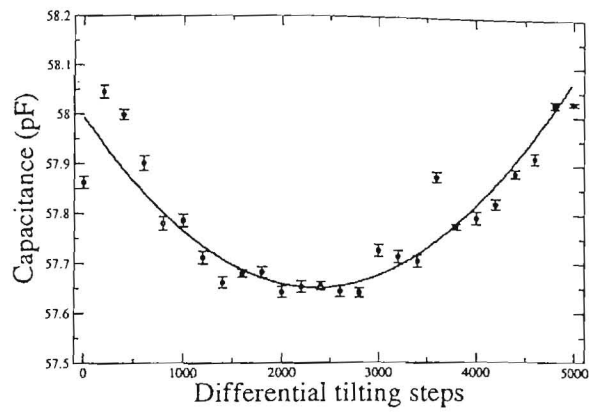


Figure 2: Assessment of the parallelization through capacitance measurements. Shown is the cylinder-plane capacitance versus the difference $\delta$ between the steps traveled by the left and right actuators in a differential mode. Each measurement is the average of 20 samples with an integration time of 1 s. The error bar represents the mean standard deviation on each data set. The measurements were performed at an average distance $d = 460\mu$m and fitted with a parabolic function as $C(\delta) = k_0 + k_1\delta + k_2\delta^2$, shown as a continuous curve, arising from the leading order term in the expansion of Eq. 3 to quadratic order in $\alpha \propto \delta$. The minimum of the curve occurs at $2500 \pm 257$ steps, settling the condition for parallelism within the fitting accuracy.

bias voltages between the cantilever and the cylindrical lens. At a given separation, the frequency of a resonant mode characterized by an effective mass $m_{\text{eff}}$ is measured both with ($\nu$) and without ($\nu_0$) the presence of the voltage. This allows for evaluation of the square frequency difference $\Delta\nu^2 = \nu^2 - \nu_0^2$, related to the voltage $V$ as:

$$\Delta\nu_{cp}^2 = -\frac{3\epsilon_0\sqrt{R}L_{\text{eff}}}{16\sqrt{2}\pi m_{\text{eff}}}\frac{V^2}{d^{5/2}}\left[\frac{\alpha^{-1}}{3(1-\alpha)^{3/2}} - \frac{\alpha^{-1}}{3(1+\alpha)^{3/2}} + \frac{\sqrt{2}}{3\pi}C\frac{d}{R}\left(\frac{\alpha^{-1}}{(1-\alpha)^{1/2}} - \frac{\alpha^{-1}}{(1+\alpha)^{1/2}}\right)\right] \tag{1}$$

where $L_{\text{eff}}$ is the effective cylinder length exposed to the cantilever (if, as in our case, the cylindrical lens is longer than the cantilever). This expression is valid in the proximity force approximation, which holds in the limit $d \ll R$, an excellent approximation in our configuration. Here $d$ is the gap separation between the cantilever and the cylinder, measured at the mid point along the axis of the cylinder. The degree of non-parallelism between the cylinder and the plane is characterized by $\alpha = (L_{\text{eff}}/2d)\sin\psi$, where $\psi$ is the tilting angle formed between the axis of the cylindrical lens and the plane. The use of a cylindrical lens rather than a full cylinder is incorporated in the coefficient $C = \frac{1}{12}\cot(\theta_w/2)(3+2\cot^2(\theta_w/2)) - \pi/4\sqrt{2}$ (here $\sin\theta_w = w/2R$). The correction in Eq.(1) containing $C$ is a sub-leading PFA correction, and will be discarded in what follows (for our cylindrical lens $Cd/R = 0.05$ for a typical separation $d/R = 10^{-3}$). The remaining correcting factor due to non-parallelism (first two terms in Eq.(1)) has a quadratic dependence on $\alpha$, given as $1 + 35\alpha^2/24$, valid for small tilting angles $\alpha \ll 1$.

The issues arising from the finite degree of non-parallelism can be disentangled from other systematic sources of inaccuracy by independently calibrating the apparatus using a spherical lens. Our spherical lens has a radius of curvature $R = 30.9$mm (with tolerance $\pm 0.5\%$), and diameter $a = (8.00 \pm 0.25)$mm. In this case, the frequency shift due to the electrostatic force between the cantilever and the spherical lens is, within PFA, given by

$$\Delta\nu_{sp}^2 = -\frac{\epsilon_0 R V^2}{4\pi m_{\text{eff}} d^2}\frac{(1 + 2d/R - \cos\theta_m)(1 - \cos\theta_a)}{(1 + d/R - \cos\theta_a)^2}, \tag{2}$$

where $d$ is the separation between the sphere and the plane, and $\sin\theta_a = a/2R$. In this case the correction due to the use of a spherical lens with a finite aperture, instead of a full sphere, is a

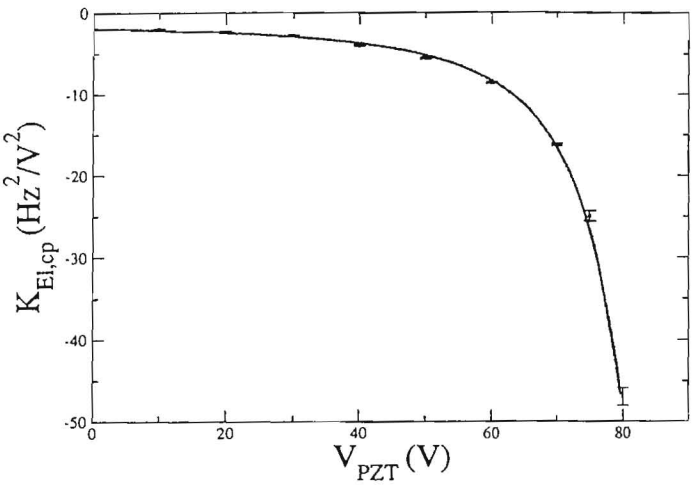


Figure 3: Electrostatic calibration in the cylinder-plane configuration. For each distance, we measure the frequency shift $\Delta\nu^2$ over a range of bias voltages $V$. The square frequency shift versus bias voltage $V$ is fitted with a function $\Delta\nu^2 = \Delta\nu^2_{\rm off} + K_{\rm El,cp}(V - V_0)^2$, as expected from Eq.(1), where $\Delta\nu^2_{\rm off}$ is an offset due to spurious background. This results in the coefficients $K_{\rm El,cp}$ appearing in the plot, with the error bars resulting from the fit. Finally, fitting $K_{\rm El,cp}$ versus the voltage $V_{\rm PZT}$ applied to the piezoelectric actuator moving the cylinder to approach the cantilever allows us to evaluate the effective mass of the cantilever and the distance offset $d_0$. The fit yields $m_{\rm eff} = (2.9 \pm 0.8) \times 10^{-3}$ kg, nearly twenty times the physical mass, and a $d_0 = (1.8 \pm 0.1)\mu$m. This discrepancy by more than one order of magnitude between the effective mass and the physical mass is attributable to the low precision of the calibration, due to relatively large $d_0$ and the corresponding small frequency shifts that do not allow for stringent constraints on the parameters.

sub-leading PFA correction, approximately equal to 0.1% for a typical separation of $d = 1\mu$m, and will be discarded in the following considerations. Therefore, we can simply replace the second factor in Eq. 2 by its leading PFA contribution, equal to 1.

Three factors play a crucial role in the analysis of the calibration data. First, the actual voltage difference experienced between the two conducting surfaces in general differs from the applied voltage due to the possible presence of residual potentials, such as Volta potentials. This can be taken into account by fitting the calibration curves with an extra parameter $V_0$ such that $V$ is superseded by $V - V_0$. Second, although we can determine the relative change in the distance quite precisely by means of the piezoelectric actuators (which have an actuation coefficient $\beta = (100 \pm 10)$ nm/V), the absolute distance between the two surfaces is not known a priori. This has to be taken into account by introducing a distance offset $d_0$, such that the absolute gap is $d_0 = \beta(V^{\rm max}_{\rm PZT} - V^{\rm closest}_{\rm PZT})$, where $V^{\rm max}_{\rm PZT}$ is a fitting parameter, representing the voltage required to make a zero gap, corresponding to a diverging frequency shift, and $V^{\rm closest}_{\rm PZT}$ is the highest voltage applied to the PZT during the run, corresponding to the smallest gap. In this way the absolute distance for a generic voltage $V_{\rm PZT}$ will be $d = d_0 + \beta(V^{\rm closest}_{\rm PZT} - V_{\rm PZT})$. Third, since the frequency of the resonator drifts due to fluctuations of ambient temperature, we measure the bare (*i.e.* without the external potential $V$) frequency before and after a measurement in the presence of $V$. The average of the two bare frequencies $\nu_0 = (\nu_0^{\rm before} + \nu_0^{\rm after})/2$, is then used to evaluate $\Delta\nu^2$. Although the overall rate of measurements is slowed down by a factor two, this technique of averaging the frequencies protects at first order from the thermal drifts of the resonator frequency during the entire duration of a calibration run.

### *2.1 Cylinder-Plane Geometry*

The parallelism between the cantilever and the cylinder is assessed by minimizing their capacitance. Again using the proximity force approximation, the capacitance between these two bodies

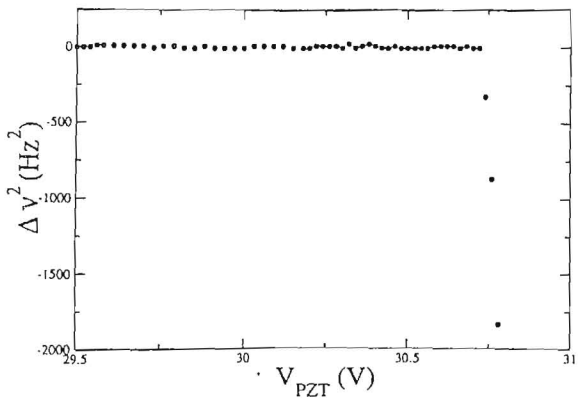


Figure 4: Observation of a strong attractive force in the cylinder-plane system. Notice the different PZT voltage scale from the electrostatic calibration shown in Fig. 3 as it results from an independent run after a readjustment of the cylinder location. The step size of approach is 10 mV, corresponding to 1 nm, and the total explored distance is 100 nm.

is given by

$$C = \frac{2\pi\epsilon_0 L_{\text{eff}}\sqrt{R}}{\sqrt{2d}}\frac{1}{\alpha}\left(\sqrt{1+\alpha}-\sqrt{1-\alpha}\right). \tag{3}$$

The tilting angle $\psi$ (and therefore $\alpha$) is experimentally controlled by operating the two motorized actuators in differential mode, attempting to keep the average distance $d$ (the separation from midpoint of the cylinder) constant through angle adjustment. The precision of the achieved parallelism is then determined by the quality of the fitting of the capacitance versus differential steps number, propagated to determine the dispersion on the number of steps at minima compatible with the fitting error. This results in a precision of about 257 step units of the motorized actuator and, since one step of the actuator corresponds to 185 nm, this translates into a displacement precision of 47$\mu$m. With the two actuators arms being spaced by 6 cm, it yields an upper bound on parallelism of $8 \times 10^{-4}$ rad. Therefore, given the width of the cantilever of 1 cm, the minimum achievable separation has an upper bound of 8 $\mu$m. The precision can be improved by minimizing stray capacitance between various contacts, since the precision of the capacitance meter is some percentage of the total capacitance in the system, usually 0.05%. An example of parallelization through capacitance measurements is shown in Fig. 2.

Once the parallelization has been achieved at the best of the available precision, we have performed electrostatic calibrations by using the piezoelectric actuator located underneath the cylindrical lens frame. In Fig. 3, the curvature coefficient of the electrostatic square frequency shift is plotted versus the PZT voltage, and fitted based on Eq. 1, assuming parallelism ($\alpha = 0$), and disregarding sub-leading PFA corrections (*i.e.* setting $C = 0$). The minimum separation achieved at 1.8 $\mu$m is presumably limited by the presence of micron sized dust particles or the defects of the surface edges, as we obtained sudden upshifts for voltages immediately higher than the rightmost point. Despite these apparent limitations in the closest gap, we did observe a strong distance-dependent attractive force as shown in Fig. 4. The observation of this attractive force cannot be attributed to the cylinder-plane Casimir force due to the apparently large gap separation where the Casimir signal is expected to be weak. Notice that $\Delta\nu^2 \simeq -2000$ Hz$^2$ at the rightmost data point in Fig. 4, and this is a factor of 40 larger than $\Delta\nu^2 \simeq -50$ Hz$^2$/V$^2$ of the rightmost data point in the electrostatic calibration shown in Fig. 3. This strong attractive behavior could be due to forces of chemical origins caused by the aforementioned defects, such as dust particles and or layers of dielectric contaminants in which local van der Waals interactions or an electrostatic force of residual charges cannot be neglected. To simplify this complex situation

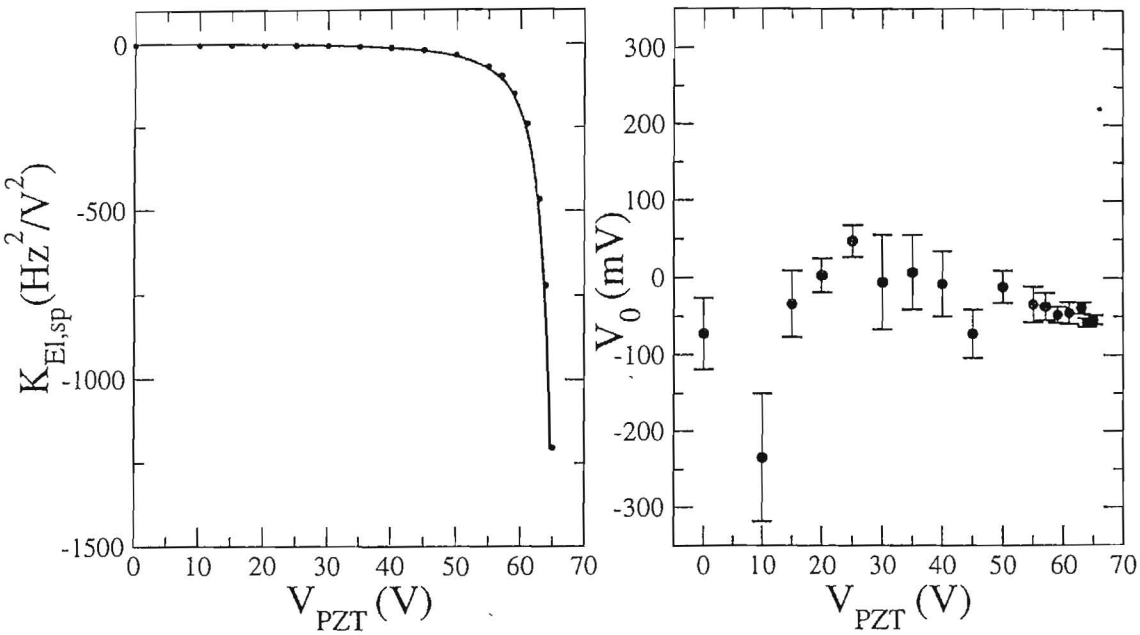


Figure 5: Electrostatic calibration for the sphere-plane configuration (left) and dependence of $V_0$ with respect to the distance (right). The rightmost data point is taken at 65 V (corresponding to 330 nm of the minimum separation gap based on the value of $V_{PZT} = (68.3 \pm 1.0)$V from the fit). The determination of the residual potential $V_0$ from the fit becomes progressively better as the two surfaces get closer, reaching the precision of 6 mV at the closest distance, to be compared with the large dispersion of the data al large distances.

surrounding the cylinder-plane analysis, we have studied the sphere-plane configuration with the same measuring apparatus and cantilever beam.

### *2.2 Sphere-Plane Geometry*

For the sphere-plane geometry, a plano-convex spherical lens with radius of curvature $R = 30.9$ mm (tolerance 5%) and diameter $a = (8.0 \pm 0.25)$ mm is coated with 250 nm layer of gold. Electrostatic calibrations for this configuration are performed as shown in Fig. 5, where $K_{El,sp}$ at each piezoelectric voltage (left) is plotted versus the PZT voltage along with a residual potential $V_0$ obtained from the corresponding fitting (right), based on the leading PFA contribution in Eq. 2. It is evident that the separation gap between the two surfaces is greatly reduced, with the frequency shift reaching as large as -1200 $Hz^2/V^2$ at an estimated gap of 330 nm compared to the highest frequency shift of -50 $Hz^2/V^2$ at an estimated gap of 1.8 $\mu$m in the cylinder-plane case. The electrostatic calibration in this close approach also allows us to better evaluate the effective mass of the cantilever, which yields $m_{\text{eff}} = (1.6 \pm 0.3) \times 10^{-4}$ kg, quite close to the physical mass of the cantilever. The determination of $V_0 = -(55 \pm 6)$mV gradually converges as the separation gap is decreased. In the same run, from the rightmost point corresponding to the minimum gap explored with the electrostatic calibration, we have continued the data acquisition by applying a counterbias equal to $V_0$ and increasing the distance resolution to the smallest distance increment allowed by the voltage supply unit driving the piezoelectric actuator, a minimum voltage increase of 10 mV. Fig. 6 shows a plot of $\Delta\nu^2$ versus distance right before hard contact, with a systematic downshift in the frequency being evident at decreasing distances. In the proximity force approximation, the frequency shift due to the Casimir force is given by

$$\Delta\nu^2_{\text{Cas},sp} = -\frac{\pi\hbar c R}{480 m_{\text{eff}}}\frac{1}{d^4} = -K_{\text{Cas}}\frac{1}{d^4}, \tag{4}$$

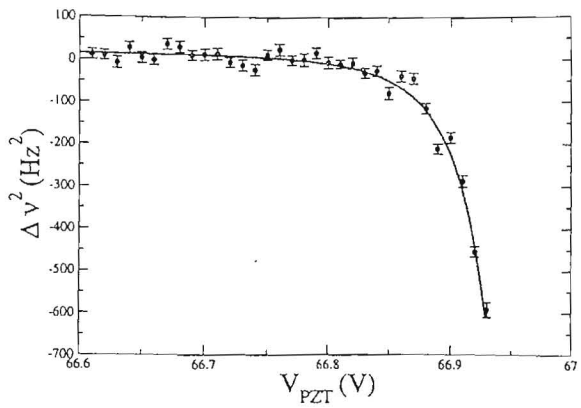


Figure 6: Observation of a downshift in a run with the sphere-plane configuration and a counterbias voltage $V = +55\text{mV} = -V_0$ canceling, at leading order, the Volta potential $V_0$. This measurement has been taken sequentially to the electrostatic calibration shown in Fig. 5. Each point was taken every 20 mV of applied PZT voltage corresponding to 2 nm right before the hard contact at 66.93 V. Error bars corresponding to few mHz result from the error in the fitting of the resonance curve of the cantilever.

where we have discarded sub-leading PFA corrections due to the finite aperture of the spherical lens. Using $m_{\text{eff}} = 1.6 \times 10^{-4}$ kg, the coefficient in Eq.(4) predicts $K_{\text{Cas}} = -(4.0 \pm 0.8) \times 10^{-26}$ $\text{Hz}^2\text{m}^4$, while the coefficient from the best fit with Eq.(4) gives $K_{\text{Cas}} = -(8.1 \pm 3.2) \times 10^{-30}$ $\text{Hz}^2\text{m}^4$ and $d_0$ corresponding to $V_{\text{PZT}} = 66.93\text{V}$, which is four orders of magnitude smaller than the theoretical prediction. If, instead, we fix the value of $d_0$ corresponding to $V_{\text{PZT}} = 68.3\text{V}$ as obtained from the electrostatic calibration, the discrepancy in the coefficients between theory and experiment is reduced to within a factor of two, remarkably close considering the quoted 10% uncertainty in the actuator coefficient and its propagation in the distance dependence of the force, showing how critical the determination of $d_0$ is. The electrostatic calibration provides a superior determination of $d_0$ since it is obtained from a broader range of distances (over 6 $\mu$m) and the minimized dispersion of the frequency shifts cancels most of the thermal drifts as described above. At variance with this, the determination of $d_0$ from the measurement at close gaps and with a counterbias runs has a distance range of only 100 nm and is completely vulnerable to the thermal drift. In future runs, we will study extensively the reproducibility of the curves accumulating at the same time more statistics to verify under which conditions the discrepancy between the two determinations of $d_0$, from the electrostatic calibrations and from counterbias (Casimir-seeking) runs, can be minimized.

## 3 Conclusion

We have reported the current status of our experiment on the Casimir force in cylinder-plane and sphere-plane geometries. A key advantage of the cylinder-plane geometry is the larger distance range over which we can observe the Casimir force. The performances of our apparatus seem limited by the thermal drifts which result in fluctuations of the resonance frequency of the cantilever and drifts in the absolute distance between the curved and the flat surfaces. Electrostatic calibrations have been successfully performed in the sphere-plane configuration and have shown convergence of the estimated parameters such as the Volta potential and the distance offset which can be then determined with order of 1 % precision.

## Acknowledgments

We thank J. Harris and J. H. Brownell for many valuable suggestions, and R. Johnson for skilful machining work.

## References

1. H.B.G. Casimir, Proc. K. Ned. Akad. Wet. B **51**, 793 (1948).
2. Y.B. Zeldovich, Sov. Phys. JETP **6**, 316 (1967).
3. S.Weinberg, Rev. Mod. Phys. **61**, 1 (1989).
4. S.M. Carroll, Living Rev. Rel. **4**, 1 (2001).
5. E. Fischbach and C.L. Talmadge, *The Search for Non-Newtonian Gravity* (AIP/Springer-Verlag, New York, 1999).
6. S.K. Lamoreaux, Phys. Rev. Lett. **78**, 5 (1997); U. Mohideen and A. Roy, Phys. Rev. Lett. **81**, 4549 (1998); H.B. Chan, *et al.*, Science **291**, 1941 (2001); G. Bressi, *et al.*, Phys. Rev. Lett. **88** 041804 (2002); R.S. Decca, *et al.*, Phys. Rev. Lett. **91**, 050402 (2003).
7. M.J. Sparnaay, Physica **24**, 751 (1958); P.H.G.M. van Blokland and J.T.G. Oveerbeek, J. Chem. Soc. Faraday Trans. I **74**, 2637 (1978).
8. G. Plunien, B. Müller, and W. Greiner, Phys. Rep. **134**, 87 (1986).
9. P. Milonni, *The Quantum Vacuum* (Academic Press, San Diego, 1994).
10. S.K. Lamoreaux, Rep. Prog. Phys. **68**, 201 (2005); R. Onofrio, New J. Phys. **8**, 237 (2006).
11. E.M. Lifshitz, Zh. Eksp. Teor. Fiz **29**, 94 (1956) [Sov. Phys. JETP **2**, 73 (1956)]; E.M. Lifshitz and L.P. Pitaevskii, Statistical Physics, Part 2 (Butterworth-Heinemann, Oxford, 2002).
12. See for instance the Focus Issue on Casimir Forces, in New Journal of Physics, October 2006.
13. A. Lambrecht, V.V. Nesvizhevsky, R. Onofrio, and S. Reynaud, Class. Quant. Gravity **22**, 5397 (2005).
14. D.A.R. Dalvit, F.C. Lombardo, F.D. Mazzitelli, and R. Onofrio, Europhys. Lett. **67**, 517 (2004).
15. M. Brown-Hayes, D.A.R. Dalvit, F.D. Mazzitelli, W.J. Kim, and R. Onofrio, Phys. Rev. A, **72**, 052102 (2005).
16. T. Emig, R.L. Jaffe, M. Kardar, and A. Scardicchio, Phys. Rev. Lett. **96**, 1 (2006); M. Bordag, Phys. Rev. D **73**, 125018 (2006); H. Gies and K. Klingmuller, Phys. Rev. Lett. **96**, 220401 (2006); D.A.R. Dalvit *et al.*, Phys. Rev. A **74**, 020101(R) (2006); A. Rodriguez *et al.*, E-print arXiv: 0704.1890v2 [physics.comp-ph] 18 April 2007.
17. B.V. Derjaguin and I.I. Abrikosova, Sov. Phys. JETP **3**, 819 (1957); B.V. Derjaguin, Sci. Am. **203**, 47 (1960).
18. J. Blocki, J. Randrup, W.J. Swiatecki, and F. Tsang, Ann. Phys. **105**, 427 (1977).
19. T. Kouh, O. Basarir, and K.L. Ekinci, Appl. Phys. Lett. **87**, 113112 (2005).